Thin Solid Films 738 (2021) 138960

Contents lists available at ScienceDirect

Thin Solid Films

journal homepage: www.elsevier.com/locate/tsf

Effect of nanoscopic defects on barrier performance of thin films deposited by plasma-enhanced atomic layer deposition on flexible polymers

Réka Lilla Kovács [a,*], Szilvia Gyöngyösi [a], Gábor Langer [a], Eszter Baradács [c,a], Lajos Daróczi [a], Péter Barkóczy [b], Zoltán Erdélyi [a]

[a] Department of Solid State Physics, Faculty of Sciences and Technology, University of Debrecen, H-4002, Debrecen, Bem tér 18/b, Hungary
[b] FUX Zrt., H-3527, Miskolc, Besenyői u. 8., Hungary
[c] Department of Environmental Physics, Faculty of Sciences and Technology, University of Debrecen, H-4026, Debrecen, Poroszlay u. 6, Hungary

ARTICLE INFO

Keywords:
Plasma-enhanced atomic layer deposition
Mechanical stability
Thin film cracking
Gas transport properties
Mass spectrometry
Numerical simulations

ABSTRACT

Penetration paths caused by nanoscopic defects in plasma-enhanced atomic layer deposited (PEALD) Al_2O_3 thin films could increase their transmission rate, mechanical limitations could impair their encapsulation utility. In contrast, this phenomenon could be beneficial in the case of polymer electrolyte fuel cells containing a proton exchange membrane, where water retention in the membrane is crucial for efficient transport of hydrated ions. Nanocracks in the deposited layer can act as nanovalves at low humidity levels and maintain the suitable level of hydration for the membrane. This paper presents the results of a unique, in situ oxide film cracking-gas permeation measurements on 25–100 nm Al_2O_3 coated low-density polyethylene. The developed measurement chamber enables the bulging of the substrate/coating system, which initiates the cracking of the coating. Under the same mechanical load, the permeability decreases exponentially with film thickness: quadrupling the film thickness reduced it by a tenth. Simulation-based empirical models on gas diffusion through defected barrier layers are summarized, and an analytical model is constructed instead. We have also carried out simulations to help understand the processes. The derived analytical equations perfectly describe the literature data, our simulations, and experimental results. The introduced technical setup, experimental and theoretical work may open further perspectives in understanding the behavior of barrier layers under mechanical loading.

1. Introduction

Polymeric materials are the most suitable substrates for flexible electronics, solar cells, furthermore, these materials play a significant role in advanced packaging systems [1]. Modified atmosphere packaging techniques of food products – in which altered atmosphere is created in the headspace that retards chemical deterioration while simultaneously retarding growth of spoilage organisms – are being developed in order to improve the performance of packaging systems i.e., shelf-life extension, cost-efficiency and consumer convenience. When considering technological development, one of the main challenges that must be overcome is the weak barrier, inappropriate gas transport properties of polymers to water vapor and gasses. Carbon dioxide (CO_2) permeability of packaging materials plays an important role in the preservation purposes as it is nontoxic and has a bacteriostatic effect [2–5].

To upgrade content protection and extend the shelf-life of a given product, thin oxide films often used as functional and protective coating on the top of the packaging material [6–11]. Plasma-enhanced atomic layer deposition (PEALD) is an excellent technique to cover these temperature-sensitive substrates with densely packed, virtually defect-free, highly uniform films which gives the possibility to enhance gas and water vapor diffusion barrier properties [12–18]. The plasma-enhanced method utilizes plasma in the ALD reaction chamber to generate highly reactive, energetic species, which enables the deposition of a wide range of materials (see Reference [13]) with outstanding physical and chemical characteristics. Among these Al_2O_3 is one of the most intensively examined diffusion barrier layer.

In those fields of applications where flexibility is a criterion the mechanical stability of the deposited passivation layer is especially important, i.e., in thin film encapsulation of organic light-emitting diodes (OLED) [19–23]. Penetration paths caused by thin film cracking increase the water and gas transmission rate of ultra-barriers, consequently, this must be considered when thin film coated flexible

* Corresponding author.
E-mail address: kovacs.reka@science.unideb.hu (R.L. Kovács).

https://doi.org/10.1016/j.tsf.2021.138960
Received 2 June 2021; Received in revised form 4 October 2021; Accepted 8 October 2021
Available online 10 October 2021

substrates are required to bend, flex or roll during production or end use [24–35]. In contrast, this phenomenon could be beneficial in the case of polymer electrolyte fuel cells containing a proton exchange membrane, where water retention in the membrane is crucial for efficient transport of hydrated ions. Like the way cactus retains water in arid conditions, nanocracks on the deposited hydrophobic layer can swell in humidified conditions or become narrower in anhydrous conditions reduce the water loss. These cracks can act as nanovalves at low humidity levels and maintain the suitable level of hydration for the membrane [36,37].

Recently, numerous studies reported improved barrier characteristics of single oxide layers by optimizing the deposition conditions, including deposition temperature, type of the plasma gas, plasma power, pulsing and purging times, electrode-substrate distance etc. to achieve lower transmission rates [38–46]. Prolonged diffusion paths can be obtained by applying multilayers, nanolaminates of different materials on flexible substrates. Structures built by altering inorganic ALD layers showed enhanced mechanical properties which resulted in better barrier performance during tests [47–57]. By combining the brittle metal oxides with organic films (Vitex technology) one can inhibit the propagation of defects through the composite system, as the organic layer serves as a stress buffer layer and creates a tortuous path for the diffusing species. With these techniques research groups getting closer to the required values for OLED encapsulation, water vapor transmission rate less than $10^{-6}\,g\,m^{-2}d^{-1}$ and oxygen permeability lower than $10^{-3}\,cm^3\,m^{-2}\,d^{-1}$ [19,58–68].

In the case of ultra-barriers, the measurement of water vapor and gas permeabilities with Mocon and Brugger devices suffers from sensitivity problems. They detect the permeated molecules with a coulometric and with a piezoresistive pressure sensor. The lower detection limit of these detectors does not meet the abovementioned requirements for OLED encapsulation [11,19,69–71]. The Ca test method is a more precise and sensitive technique. Upon exposure to water vapor and oxygen the conductive and opaque Ca metal becomes non-conducting and more transparent. At room temperature the oxidation is mainly attributed to water, so by observing the electrical or optical changes the effective permeability can be determined. The latter allows to determine effective water vapor transmission rates as low as $3 \times 10^{-7}\,g\,m^{-2}\,d^{-1}$ [19,72]. Another accurate technique to verify water and gas barrier properties of thin film coated polymers is mass spectrometry. Quadrupole mass spectrometry (QMS) provides high sensitivity (ppb levels) with short measurement times. Uniquely, it gives the opportunity for simultaneous determination of permeabilities of gas mixture components with different mass to charge (m/z) ratios, since it measures the permeant partial pressure instead of the total pressure within the system [73–78].

The failure mode of brittle thin film structures on flexible substrates, such as channeling/cracking, buckling or delamination at interfaces, predominantly depends on the mechanical properties of the substrate, the adhesion between the substrate and its surface coating, and thin film thickness and cohesion [79]. In the case of nanofilms, the visualization, characterization and interpretation of this failure mode, and revealing the consequence of the evolved defects, for example, the effect of cracks on permeation could be quite challenging. Fragmentation testing is an experimental approach based on the study of the cracking dynamics, the analysis of the progressive failure of the brittle coating under stress. During uniaxial tensile testing, parallel cracks perpendicular to the load direction appear and propagate until the density of these cracks reaching saturation as the nominal strain increases. This saturation crack density is related to the interfacial shear strength, i.e., the adhesion of the layer [24,80–84]. Bulge testing is a 2D biaxial fragmentation test, which is a very efficient way to examine the mechanical performance of thin films on compliant polymers, as it provides a more precise reflect of the actual multiaxial stress state conditions during fabrication, conversion processes, and in the end-use. Mechanical properties of oxide films can be deduced by imposing the coated membrane to uniform pressure. Recording the pressure-corresponding out-of-plane deflection data the residual stress in the coating layer, elastic modulus, and other important parameters such as yield strength and fracture toughness can be calculated [84–91]. A common methodology to study the effect of deformation on flexible electronic devices is the bending test, when the coated polymer is bending around a cylinder of a given radius r. Varying this radius different strain rates, and according to this, different crack patterns can be achieved [21,25,57,63,92]. Two major advantages associated with bulge test are the simplicity of specimen handling (re-clamping, re-gasketing is not needed) and the capability of imposing loading conditions. These advantages are peerless compared to other thin film testing methods such as nanoindentation, bending test technique or tensile testing [84–91].

The monitoring of the cracking mechanism can be performed either by scanning electron microscopy (SEM), atomic force microscopy (AFM), optical or acoustic techniques. This inspection on the mechanical stability of films can be done separately or parallel with transmission rate measurements [22,24,25,32,80,93–99]. Even in the case of parallel measurement techniques, movement, or re-clamping of the samples between each step are needed, which causes uncontrollable mechanical changes in the substrate/coating systems [80].

Nowadays, because of the increasing use of flexible devices there is further pretension to investigate the influence of mechanical stability on gas barrier properties of thin films, especially which were deposited by atomic layer deposition, due to their superior barrier characteristics. Very few studies have explored the mechanical properties of layers prepared by plasma enhanced atomic layer deposition, even less papers are available about how this could influence the barrier behavior. The works dealing with the correlation between the defectiveness of the barrier layer and the gas permeability are, for the most part, theoretical; there are hardly any experimental articles in the literature which combine in situ cracking of the layers during the gas transmission tests with detailed numerical calculations. For this very reason, in this work, we performed gas transmission tests combined with in situ cracking of the layers. Moreover, we integrate the effect of „intrinsic" defects in the PEALD layers, such as pinholes, and the influence of in situ cracking of thin oxide layers based on experimental data into computer simulations to show how these complex defect structures can alter the barrier usefulness.

2. Background

Gas permeation through a membrane is a two-step process i.e., the solution of the permeant in the membrane and then the diffusion of the dissolved molecules. After the absorption process in the surface layer of the membrane, due to the driving force, which is the concentration/partial pressure gradient, molecules diffusing into the material. On the low concentration/partial pressure side they desorb into the gas phase. After a certain time, a steady state of flux through the homogenous membrane is reached, and the permeability coefficient (P) can be written as the product of the diffusion coefficient (D) and solubility coefficient (S):

$$P = DS = \frac{Qd}{At\Delta \mathrm{p}} \tag{1}$$

where Q is the quantity of permeant per unit time, t, referred to unit film thickness, d, and area, A, per unit of partial pressure difference of permeant across the film, Δp. If we assume that Henry's law is valid for the process, the subsurface concentration (ρ) of the solved gas is directly proportional to the partial pressure (p) of the gas:

$$\rho = Sp \tag{2}$$

During the experiments one can determine the quantity of permeant per unit of time (Q/t) passing through the membrane with area A and thickness d [100]:

$$\frac{Q}{t} = \frac{ADSp}{\mathrm{d}} \tag{3}$$

The barrier usefulness of the ultrathin coating films clearly governed by the defects and surface imperfections. In the case of gas-barrier coated polymers, the key parameters to achieve both superior performance and cost optimization are the intrinsic resistance of the coating to thermal and mechanical loads, its thickness, and its adhesion to the substrate. To investigate the mechanical durability of the atomic layer deposited thin Al_2O_3 films under tensile and compressive strains Jen et al. [24] performed experiments on different polymeric substrates. This paper revealed that under uniaxial tensile loading the crack density and crack onset strain (critical strain for cracking) for the Al_2O_3 coatings with larger thickness is less than the crack density for the smaller thickness. The saturation crack density versus Al_2O_3 film thickness function shows $(1/h)^{1/2}$ dependency where h is the Al_2O_3 layer thickness. Furthermore, the crack onset strain (critical strain for cracking) is also higher for the thinner layers and this parameter also shows $(1/h)^{1/2}$ dependency, which also need to be considered in exploring the optimized film thickness in each application [24].

Other papers have focused on correlations between the characteristics of these defects and diffusion properties. A model on gas permeation through single- or multiple circular defects in barrier coatings were introduced by da Silva Sobrinho, Czeremuszkin, Latrèche and Wertheimer [30] This study is based on a simple geometrical approach, the total permeation flux through a single defect is the sum of the molecules that diffuse perpendicularly to the polymer surface, and molecules that traverse the wall of the defect edge and diffuse inside the polymer, and escape from the rear surface of it at unspecified locations. If a large number of defects are presented, but these are still independent holes, which means the presence of one does not influence the permeation through the other, their respective quantities of permeant are additive [30]. By further increasing the defect density this approach will not give correct results because of the overlapping of the diffusion zones of the defects. Mueller and Weisser [101] also investigated the effect of pinholes on the permeation through vacuum-coated laminate films. The introduced numerical model is valid for all pinhole sizes and takes mutual interactions between the defects into account. The transmission rate (TR) ratio is defined as the quotient of the flux for the system containing defects and the flux for the system without coating. For ordered pinhole distributions it can be calculated as follows [101]:

$$TR_{ratio} = \frac{\Theta}{1 - \exp\left(-0,432\frac{2r_0}{d_s}\right) + \Theta} \tag{4}$$

where Θ is the defectiveness of the layer $(defect\ area\ /characteristic\ defect\ spacing^2)$, r_0 is the pinhole radius, d is the thickness of the substrate/support layer. Grüniger and von Rohr [102] pointed out that with increasing defect distance the gas flow across a single defect increase, as the lateral spreading of the concentration profile is less hindered by other defects. When the distance is large enough for the concentration profiles to be considered independent of one another, the TR ratio reaches an asymptotic value, which differs for circular holes and infinitely long cracks. Hanika et al. [28] established a three-dimensional numerical simulation to reveal the effect of defect size or area (A_d) and defect spacing on permeation rate. They concluded that if the defect spacing is small, there is an interaction between the defects, which resulted in reduced concentration gradient and flux. These phenomena have strong defect size dependency, with increasing defect area the interaction is increased and appears at larger defect spacings. They introduced a predictive formula for polymer films that have coatings with different defect structures [28]:

$$TR_{ratio} = \frac{\Theta}{1 - \exp\left(-0,507\frac{\sqrt{A_d}}{d_s}\right) + \frac{\Theta}{100}} \tag{5}$$

The effect of random defect distribution on the gas permeability of multilayer films was examined by Toni et al. [103]. Ordered structures are characterized by a well-defined defect distance. The randomness of the defect distribution allows the formation of clusters of defects, which are very effective in reducing the overall permeating flux, as a result of the interaction of the concentration gradients. For higher defectiveness, the behavior of random systems become more similar to the ordered ones.

3. Numerical simulations

The time-dependent evolution of the local concentration (volume density) ρ of a gas in a polymer can be calculated by Fick's second law. If the diffusion coefficient is independent of ρ, and so also the space coordinates, Fick's second law has the following form [100]:

$$\frac{\partial \rho}{\partial t} = D\left(\frac{\partial^2 \rho}{\partial x^2} + \frac{\partial^2 \rho}{\partial y^2} + \frac{\partial^2 \rho}{\partial z^2}\right) \tag{6}$$

This equation has to be solved in three dimensions to determine the concentration distribution and then the gas flux through the polymer membrane can be calculated by using Fick's first law:

$$\vec{j} = -Dgrad\rho \tag{7}$$

Eq. (6) has to be solved under the following conditions: i) gas atoms reach the surface of the polymer only through defects (pinholes, cracks), because the oxide layer is practically impermeable, ii) the pressure is kept constant at both sides of the polymer (but they can be different), the concentration of the gas atoms in the polymer is constant on both surfaces.

In steady-state, Eq. (6) reduces to the Laplace equation and becomes independent of D:

$$0 = \left(\frac{\partial^2 \rho}{\partial x^2} + \frac{\partial^2 \rho}{\partial y^2} + \frac{\partial^2 \rho}{\partial z^2}\right) \tag{8}$$

which simplifies the calculations.

In this study, we performed numerical calculations for defects, pinholes and cracks, in ordered arrangements. Fig. 1 shows the basic parameters defining the characteristic dimensions of the defects and their distribution.

The thickness of the polymer (z-direction) is denoted by d_s, r and R are the lengths of the sides of a rectangular pinhole, l and L are the distances of the center line of the defects in the plane of the sample in the x and y-directions, respectively.

Using this parametrization, not only pinholes with $A_d = r \times R$ defect area can be simulated, but also cracks. Because if, for example $R = L$, the

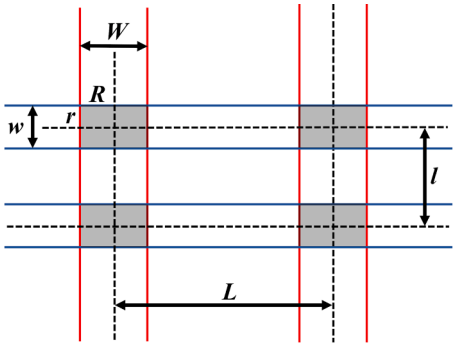

Fig. 1. Basic parameters defining the characteristic dimensions of the defects in the oxide layers and their distribution. Dark gray areas representing the rectangular pinholes, the red lines indicate parallel, and the blue lines specify the crossing cracks. The lengths of the sides of a rectangular pinhole are r and R, which become w and W when cracks are presented. L and l are the distances of the center line of the defects in the plane of the sample in the x and y directions. (For interpretation of the references to colour in this figure legend, the reader is referred to the web version of this article.)

pinholes touch with each other in the *y*-direction, resulting in cracks of width $w = r$ running in the *x*-direction, spaced l apart.

If a "cross" flag is set to true and $R = L$ and $r = l$, a crack network with a rectangular lattice geometry is formed, in which cracks of width $w = r$ run in the x direction and $W = R$ in the y direction, the center lines of which are l and L apart. This makes it possible to account for intersecting cracks, which has not been reported in the literature.

Taking advantage of the fact that the defects are identical and arranged orderly, it is sufficient to perform the calculations on only one cell of size $l/2 \times L/2 \times d$.

Eq. (8) was solved in FreeFEM using the finite element method (FEM) [104]. Starting from an isotropic mesh, we used a solution-based mesh adaptation algorithm in situ during the simulation to refine the mesh (Fig 2). The mesh was created by TetGen which is available as a plug-in FreeFEM [105].

4. Experimental methods

4.1. PEALD of thin oxide films on low-density polyethylene substrate

Commercial grade low-density polyethylene (LDPE) films with thickness of 10 μm were chosen as substrates for our permeation experiments. This material has huge relevance and popularity in the packaging industry, it has good material strength and durability, resistant to water and chemicals. LDPE is a heat-sensitive material. This fact restricts the circle of thin film deposition techniques that enables conformal and continuous coating layer preparation at low temperatures to enhance the barrier performance of the LDPE. For this reason, plasma-enhanced atomic layer deposition is one of the most appropriate method to cover the polymeric substrates with highly uniform films [10, 106–109]. The plasma-enhanced atomic layer deposition of Al_2O_3 films was performed by a Beneq TFS 200–186 reactor, equipped with a capacitively coupled radio frequency plasma processing apparatus with showerhead type electrode assembly. The equipment was operated in remote plasma mode, which means that a metal grid was placed between the powered electrode and the substrate to prevent direct contact with the plasma and the polymer surface and to suppress the harmful energetic ion damage [13]. The precursors used for thin films were trimethylaluminum (TMA, 97%, Sigma-Aldrich) and O_2 (99,999%) as an oxidizing agent. Nitrogen (99,99%) was used as a carrier and purging gas. During deposition cycles the reactor pressure was maintained around 120 Pa, the temperature was 38 °C. Plasma was produced by flowing O_2 into the reactor at 100 sccm, the plasma power was 50 W during the reactant pulse steps and 10 s O_2 plasma activation (pre--treatment) was applied before each film deposition to remove surface contamination from the LDPE surface and to enhance the formation of hydroxyl (OH) functional groups. The dose times for one deposition cycle for an Al_2O_3 film was as follows: 1) a TMA feeding for 0,15 s, 2) a N_2 purge for 2 s, 3) an O_2 feeding with 50 W RF plasma power for 2 s, and 4) a N_2 purge for 2 s. The thickness of the layers was measured by a stylus profilometer (AMBIOS XP-1, Crediton), and it was consistent within 5% relative error with the nominal thicknesses (25, 50, 75 and 100 nm).

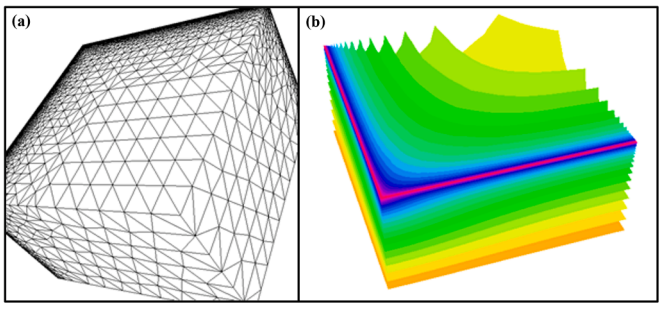

Fig. 2. An example for the mesh (a) and for the solution (b) (isoconcentration planes) for crossing cracks.

4.2. In situ measurement of the effect of cracks on the gas permeation

The schematic representation of the main parts of the permeation measurement system can be seen in Fig. 3.

Uncoated and coated polymer substrates, with sampling area of 0,0085 m^2, mounted between two chambers (separated by the sample itself) and sealed with rubber gaskets against each enclosed volume. At the beginning of the experiment, a closed butterfly valve isolates the atmospheric pressure (during the total testing time held at this value), high purity test gas, carbon dioxide (CO_2), and the analyzed sample. To remove any residual gas contamination from the two chambers and from the test piece atmospheric pressure N_2 (99,99%) gas inlets are connected. The gas flow calibrated quadrupole mass spectrometer (QMS) is coupled to the sample holding volume via a membrane inlet (SILPURAN® FILM 2030, Wacker Chemie AG, 20 μm thickness). This inlet functions as an interface between the studied film (atmospheric pressure, 101325 Pa) and the vacuum of the QMS (10^{-5} Pa), in order to avoid the pressure difference induced damage in our coating layers. The inlet has a very short response time to the gas concentration changes in its environment (compared to the coated LDPE sample), has a suitable transmission rate ($<5 \times 10^{-6}$ $cm^3\ s^{-1}$ at standard temperature and pressure), so the gas diffusion across the inlet does not vary the atmospheric pressure state of the test gas. Therefore, the changes in the ion fluxes caused by the N_2 flushing process i.e., the removal of gasses can precisely trackable with the QMS.

After the N_2 flushing/cleaning, the background signal of the test gas is registered. The experiment starts by the opening the butterfly valve, the test gas container and the sample are connected. The driving force of the diffusion process is the partial pressure difference of the test gas between the two sides of the sample, which resulted in partial pressure increases on the spectrometer side of the sample. The measured flow rate, Q (atmospheric pressure (atm)) $cm^{-3}\ d^{-1}$) is proportional to the number of diffused molecules which are permeated through the sample. From the kinetics of the process, i.e., from the estimation of time lag or by the evaluation of steady-state flow, further properties of the specimens can be derived [100].

By following the described measurement steps, we can record the spectrum for the "uncracked" film. After that, the butterfly valve and the N_2 inlet and N_2 outlet valves are closed. A buffer tank is filled with compressed air and linked with the closed N_2 inlet valve (left-hand side arrow on the figure) via a precise digital pressure gage, which is coupled to the Al_2O_3-coated face of the substrate. Then, after surely adjusted the +1000 Pa overpressure, which means 1000 N m^{-2}, by opening the N_2 inlet valve the volume between the butterfly valve and the test piece is pressurized, the thin film coated LDPE is bulged, as a result, cracking of the oxide layer took place. This over-pressurized state is held for 10 s and finished by closing the N_2 inlet and opening the N_2 outlet valve on this side of the sample. In the following step, the N_2 inlet and outlet valves are opened, the N_2 source is reconnected, and the flushing-permeability testing steps are repeated. After the 10 s over pressurization no substrate damage was observed, the gas transmission rate of the substrate did not change considerably (~ 10%), which is clearly necessary if we want to examine the effect of oxide layer cracks. Kim et al. have showed that the long-term reliability of thin film coated flexible polymers also affected by time-dependent local cracking of the polymer underneath the channel cracks [110].

Further details of the experimental setup can be found in Reference [111].

4.3. Characterization of cracked structures by scanning electron microscope (SEM)

The structure and morphology of the channel cracks were

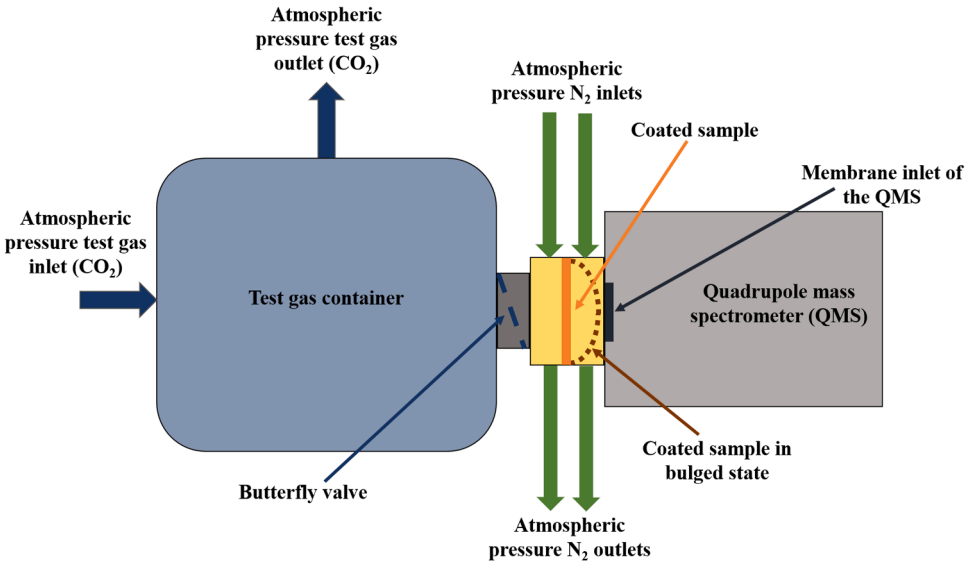

Fig. 3. The schematic drawing on the main parts of permeation measurement and in situ cracking system.

investigated by scanning electron microscopy (HITACHI S4300-CFE, Hitachi High-Technologies Europe GmbH.) after the gas permeation tests. Before the microscopic examination thin gold layer was sputtered on the surface of the samples to decrease charge buildup effects in the specimen. Seconder electrons were collected to produce images, the acceleration voltage was 15 kV, the working distance varied between 18 and 22 mm in order to get the best resolution. In order to get quantitative data, the SEM micrographs were analyzed by a quantitative computer image analyzing software [112]. The average crack area ratios (defectiveness), crack distances (L), crack widths (w) were extracted from the cracking patterns of at least 5 different pictures for each sample.

5. Results and discussion

5.1. Gas permeation measurements

The gas permeation measurements were performed with PEALD Al_2O_3 coated LDPE membranes described in Section 4.2.

The oxide layers decrease the diffusional flux of the CO_2 ($m/z = 44$) compared to the bare LDPE. Increase in the oxide layer thickness from 25 to 100 nm the flow rate decreases approximately exponential manner due to the decrease of pinhole density in the layers. After the cracking process, the fluxes increase for all layer thicknesses (Fig 4). The flux after cracking is, however, still significantly lower than the flux for the bare LDPE. This quantity provides important information about how the defects alter the transmission properties. As can be seen in Fig. 4, under the same mechanical load, the transmission rate ratio for CO_2 (CO_2TR ratio) decreases exponentially with film thickness: quadrupling the film thickness reduced it by a tenth. This implies that under the same mechanical load there is a threshold value in the coating thickness, where the barrier efficiency and cost ratio are the most beneficial.

5.2. Pinholes of the as-prepared layers

It is known that ALD prepared oxide layers are usually not defect-free but contain point-like discontinuities, so-called pinholes. If the layer is deposited under the same conditions on the same substrate, the pinhole density (η) depends primarily on the film thickness (d). In a previous study, it was found that in the case of Al_2O_3 layers with the thickness of 15–100 nm η is in the range of 1–100 cm^{-2} and depends exponentially on d [113]:

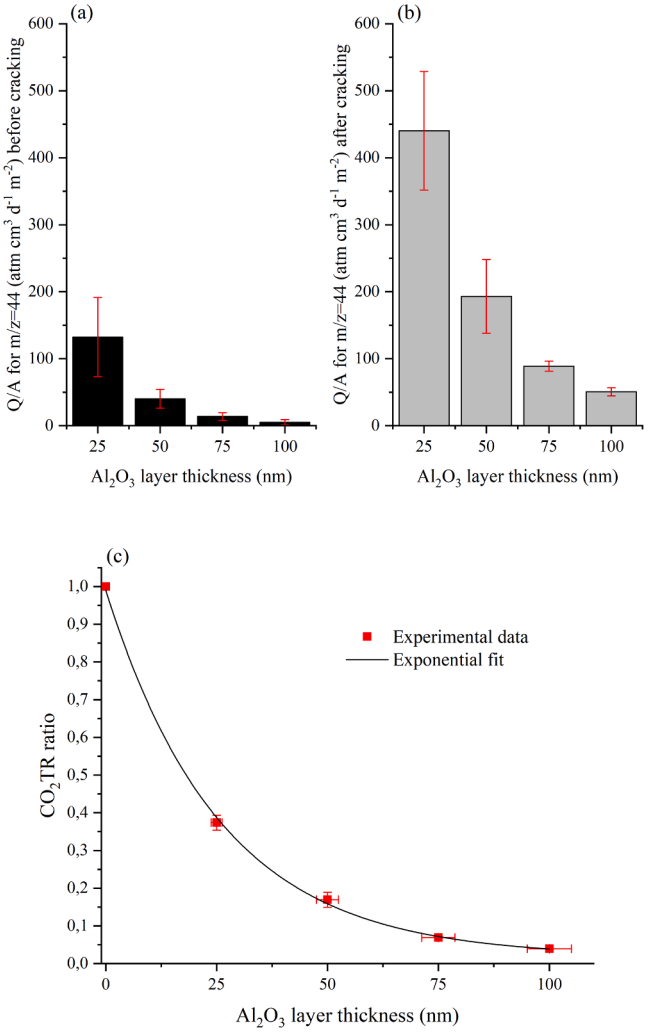

Fig. 4. Measured diffusional flux of CO_2 before (a) and after (b) the cracking process, and CO_2TR ratio (c) as a function of the Al_2O_3 layer thickness. (For interpretation of the references to colour in this figure legend, the reader is referred to the web version of this article.)

$$\eta = \eta_0 \exp(-\lambda d)$$

Fitting their experimental data, we may determine the parameters: $\eta_0 = 136\ \mathrm{cm}^{-2}$ and $\lambda = 0{,}03\ \mathrm{nm}^{-1}$.

Although our substrate is different, but we prepared the layers under similar conditions, and the thickness of our layers is in the range of 25–100 nm, we may expect that the pinhole density depends similarly on the film thickness. To verify this, assuming that the gas permeability of the layer is primarily determined by the density of the pinholes, an estimate can be made of how the CO_2TR ratio should change as a function of the layer thickness.

The gas flux through a coated substrate can be calculated as

$$j = -\frac{\Delta p}{\frac{d_s}{P_s} + \frac{d_l}{P_l}}, \tag{9}$$

where Δp is the pressure difference between the two sides of the membrane, d_s, d_l and P_s, P_l are the thickness and the permeability of the substrate (LDPE foil in our case) and the coating layer (Al_2O_3 in our case), respectively [114]. This expression can be written as

$$j = \frac{j_s}{1 + \frac{P_s}{P_l}\frac{d_l}{d_s}}, \tag{10}$$

with $j_s = -P_s \Delta p / d_s$, that is the flux through the uncoated substrate. The quotient of j and j_s from Eq. (10) is just equal to the gas transmission rate ratio. If the permeability of the coating layer is proportional to the pinhole density, $P_l = P_0 \exp(-\lambda d_l)$, where P_0 is a preexponential factor proportional to η_0, we obtain

$$\frac{j_s}{j} = \frac{1}{TR_{ratio}} = \frac{P_s}{P_0 d_s} d_l \exp(\lambda d_l) + 1 \tag{11}$$

Fig. 5 shows the reciprocal of the measured CO_2 transmission rate ratio as a function of the thickness of the oxide layer without cracks. The experimental data points were fitted with the function obtained above (Eq. (11)).

It can be seen that the fit is perfect, and the value λ obtained (0,028 nm^{-1}) shows a very good agreement with the value obtained from the data found in Reference [113]. Note that knowing the thickness of the LDPE foil (10 μm), P_s/P_0 is in the order of 10^{10}. This means that the permeability of the LDPE substrate is about 10^9 to 10^{10} times greater than that of a defect-free Al_2O_3 layer, which is consistent with the image that the gas only reaches the substrate surface through layer defects.

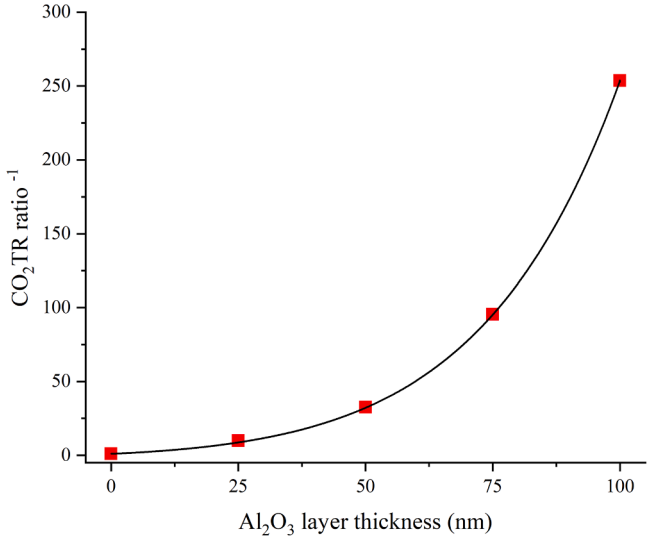

Fig. 5. The reciprocal of the measured CO_2 transmission rate ratio as a function of the thickness of the oxide layer without cracks. The continuous curve is a function given by Eq. (11) fitted to the experimental points. (For interpretation of the references to colour in this figure legend, the reader is referred to the web version of this article.)

5.3. Characterization of the crack network, defectiveness of the layers

The formed crack network in the coating layers after the over pressurization were investigated by SEM, and computer image analyzing software was also applied to get quantitative data. It is known from the literature that crack density and film thickness show a strong correlation. For example, Jen, Bertrand and George examined Al_2O_3 layers with a thickness of 5–80 nm prepared on Teflon support, which were subjected to tensile and compressive loads. It was found that the crack density is inversely proportional to the square root of the Al_2O_3 layer thickness [24].

After the cracking procedure, the results of the analysis of the electron microscopic images (an example shown in Fig. 6) of our layers are shown in Fig. 7 and in Table 1. The proportionality found by Jen, Bertrand and George is also met in our case, the thinner film has higher crack density, and the latter scaled as $(1/h)^{1/2}$, which also ensures that the applied strain is sufficient to reach saturated crack densities.

Table 1 also contains the defectiveness of the Al_2O_3 layer. However, this is not a complete defectiveness, as the pinholes already present in the initial layer also have a contribution. This contribution can be estimated from Eq. (4) if the size of the holes is known. Furthermore, we took into account that the channeling cracks are V-shaped [111]. This means that by SEM we observe higher percentages of defectiveness, than what is actually presented in the oxide layer. From the focused ion beam analysis of the cracks, we found that the crack width measured at the top of the gold coating layer–required for SEM analysis of the samples–is about twice the width of the crack measured at the polymer surface. Table 1 shows the values measured at the top of the gold layer. In the computer simulations, however, half of these were used.

However, we could not identify pinholes during SEM analyses. But since cracks 100–200 nm wide could be identified with certainty, pinholes of at least the same diameter (i.e., $r = 50$ nm) would have been found for sure. Therefore, pinholes are definitely smaller than that. The results that can be found in Reference [115] confirm this, they observed pinholes with a diameter of ca. 25 nm in Al_2O_3 layers grown on the surface of HDPE by ALD [115]. It is worth noting that the authors found that in the case when HDPE was treated with oxygen plasma prior to deposition, pinholes could no longer be observed. We also treated the LDPE foil with oxygen plasma, which may have contributed to the pinholes being so small. Note that in a previous paper, we studied the effect of plasma (oxygen, nitrogen, and oxygen-nitrogen mixture) treatment on the LDPE film [116].

Considering all this, we can safely state that the radius of the pinholes is not greater than 50 nm. Substituting this value into Eq. (4), an upper limit can be estimated for the defectiveness of the Al_2O_3 layer resulting from the pinhole contribution. This value can also be found in Table 1.

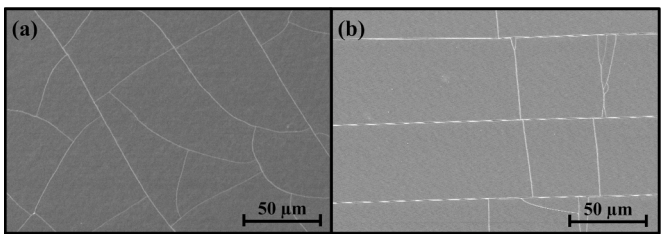

Fig. 6. SEM pictures of (a) a 50 nm thick Al_2O_3 layer after the cracking procedure and (b) cracks in a 75 nm thick Al_2O_3 layer.

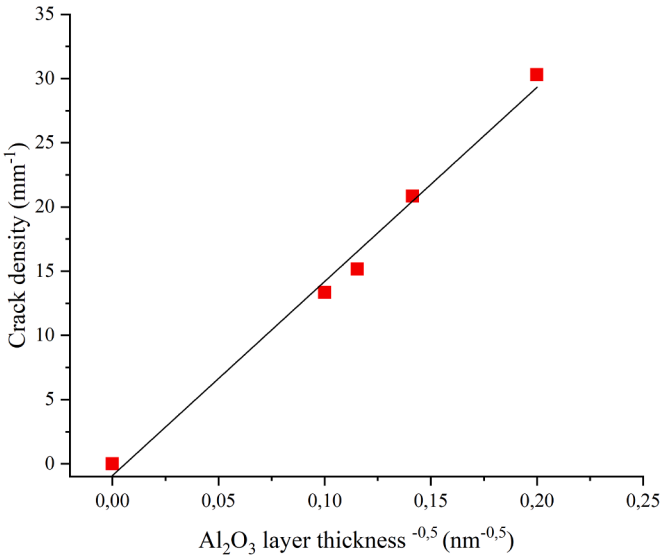

Fig. 7. Crack density as a function of the inverse of the square root of the Al_2O_3 layer thickness. The straight line is a linear function fitted to the experimental points.

Table 1
Film thickness (d_l), average crack distance (L), crack width (w), moreover the defectiveness of the film originating from cracks and pinholes. The uncertainty values of L and w were calculated as the absolute deviation from the average.

d_l (nm)	L (μm)	w (nm)	Defectiveness (%)	
			cracks	pinholes
25 ± 1,25	33 ± 2	167 ± 25	2,46	0,049
50 ± 2,50	48 ± 4	202 ± 23	1,66	0,014
75 ± 3,75	66 ± 8	196 ± 19	1,39	0,005
100 ± 5,00	75 ± 10	230 ± 41	1,23	0,002

5.4. Gas transmission rate ratio versus defect distance – simulation and theory

Very few studies have explored the mechanical properties of layers prepared by plasma enhanced atomic layer deposition, even less papers are available about how this could influence the barrier behavior. The works dealing with the correlation between the defectiveness of the barrier layer and the gas permeability are, for the most part, theoretical; there are hardly any experimental articles in the literature.

It is common in these works to represent the gas transmission rate ratio as a function of the distance of the layer defects. These defects are, in fact, almost exclusively pinholes. Fig. 8 shows the CO_2TR ratio as a function of the average crack distance for our layers.

If we want to understand the relationship between the CO_2TR ratio and the crack network, perhaps we should start by understanding the results of the computer simulations of Grüniger and von Rohr [102]. They calculated the gas flow rate J through the defect area A_d by integration of the flux j, and related J to J_{1D}, where J_{1D} represents the gas flow rate through the defect in the one-dimensional case, i.e., the flow rate through the area A_d if the barrier layer was absent. Grüniger and von Rohr calculated J/J_{1D} for uniform pinholes and parallel running cracks (no crossing cracks) distributed with constant distance to each other. To compare their results with experimental results and those of other authors, e.g. Mueller and Weisser, the J/J_{1D} should be converted to the gas transmission rate ratio [101]. The gas transmission rate ratio can be calculated by multiplying J/J_{1D} by the defectiveness Θ. Fig. 8 shows the gas transmission rate ratio as a function of the defect distance for pinholes and parallel cracks when the thickness of the polymer substrate is 100 times greater than the size of the defects (diameter of pinholes or

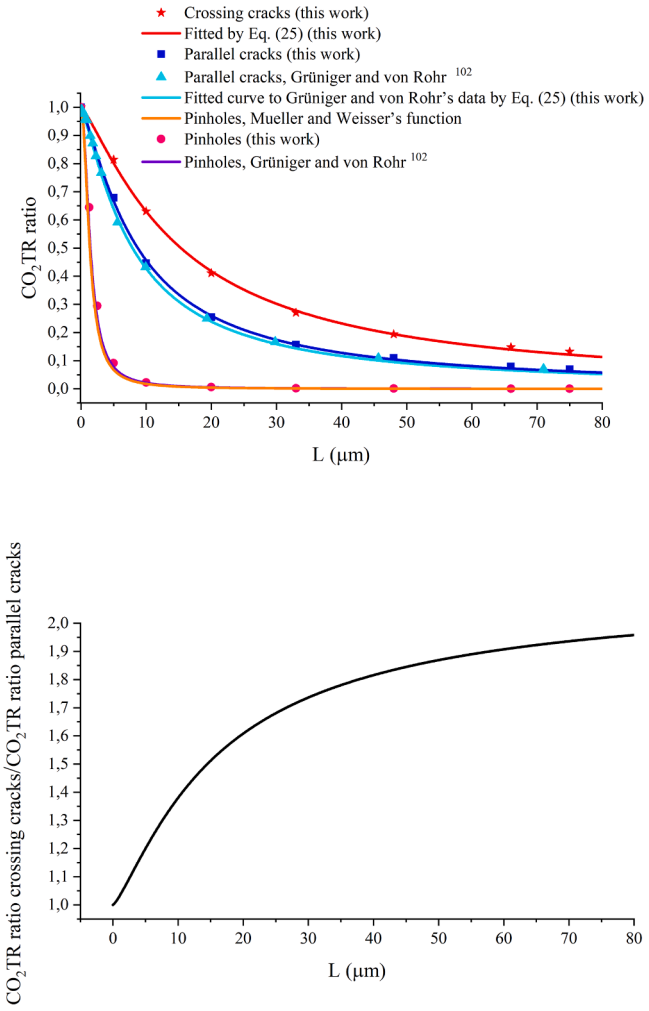

Fig. 8. CO_2TR ratio as a function of the defect distance for pinholes, parallel cracks and crossing cracks; data points show results of numerical simulations (literature and this work). Fits to pinhole data from this work are calculated with Mueller and Weisser's function (Eq. (4)) and using the simulation parameters used by Grüniger and von Rohr [102], and using Eq. (25) deduced in this work (see later in the text). Fits to crossing and parallel cracks obtained experimentally in this work and by simulation in [102] are also fitted using Eq. (25). in (a). The calculated ratio of CO_2TR ratios obtained for crossing and parallel cracks is presented in (b).

width of the cracks) converted from the J/J_{1D} data published by Grüniger and von Rohr.

To compare the results of Grüniger and von Rohr and Mueller and Weisser, we plotted the curve calculated from Mueller and Weisser's function for pinholes given by Eq. (4). As can see, the curve fits the data points perfectly (Fig. 8).

To test our computer code, we ran it with the same parameters as Grüniger and von Rohr [102]. The data points obtained fit perfectly with Grüniger and von Rohr's data points both for pinholes and parallel cracks–and so Mueller and Weisser's function (Eq. (4)) for pinholes, too [101].

To explore how crossing cracks affect the gas transmission rate ratio, we also simulated crack networks with a rectangular lattice geometry. As expected, the gas transmission rate ratio, in this case, is significantly higher than in the case of parallel cracks only. Data points obtained for the geometry of a square crack network, in this case the distances between the cracks in the x and y directions are equal ($l = L$), are also shown in Fig 8. Note that although the surface area of the cracks (Θ) is two times larger in the case of crossing cracks ($\Theta = 2w/L$) than in the

case of parallel cracks ($\Theta = w/L$), the ratio of the gas transmission rate follows a different trend. When L is small, the ratio of the two cases i.e. two datasets (see Fig. 8(b)) is close to one. With increasing defect distances this proportion also increases and approaches two-fold. This is consistent with the image that the more the diffusion fields overlap, the more the overall permeating flux is reduced.

Mueller and Weisser found Eq. (4) by fitting the results of numerical simulations. In this manner the function form was not based on any model. In the following, we will try to determine how the gas transmission rate ratio can depend on the defect distance, based on a simple model.

Consider two membranes, one continuous and permeable to gas molecules (the polymer substrate in the experiments) and the other made of a material that is impermeable to gas molecules (the metal oxide barrier layer in the experiments). Thus, a laminate made from these will only allow gas molecules to pass through if the barrier layer contains continuity defects (e.g., pinholes). Assume that the gas molecules passing through the barrier layer containing pinholes can be evenly distributed at the interface of the two membranes and then diffuse through the polymer substrate. For the sake of clarity and simplicity, Fig. 9 shows this as if the two membranes were not in contact with each other, but of course, it can also be said that the gas molecules diffuse significantly faster laterally at the interface between the oxide layer and the polymer than into the polymer.

The first phase of the process can be described as effusion. The flux of gas molecules passing through a hole is proportional to the difference in pressure on both sides of the membrane ($p_2 - p_1$):

$$j_d = E(p_2 - p_1) \tag{12}$$

E is the proportionality, or we may call it effusion coefficient. Thus, the number of gas molecules passing through the barrier layer per unit time is:

$$\frac{Q_l}{t} = j_d N_d A_d, \tag{13}$$

where N_d is the total number of pinholes. The effective flux across the defected coating layer is obtained by dividing Q/t by the total surface area A:

$$j_l = E\eta A_d(p_2 - p_1) \tag{14}$$

The second phase of the process can be described as diffusion through the polymer substrate, i.e., the flux of the diffusing gas molecules can be calculated as follows:

$$j = P_s\frac{p_3 - p_2}{d_s} \tag{15}$$

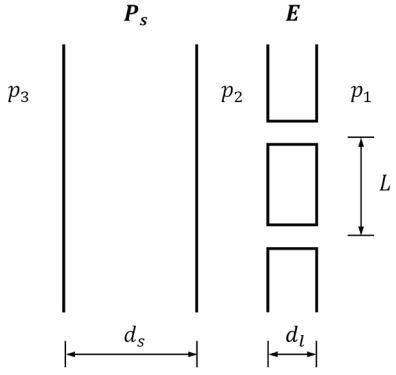

Fig. 9. Schematic drawing on a substrate (with thickness d_s), and on the top of that a coating layer (d_l) system indicating the interface between them (deliberately drawn non-connected). The permeation process through this can be described by effusion and diffusion phases.

In the steady state, the number or concentration of gas molecules at the interface between the barrier layer and the polymer support are constant, that is $j_l = j$. Considering that there is a vacuum on the polymer side, i.e., $p_3 = 0$, we obtain that:

$$p_2 = \frac{1}{1 + \frac{P_s}{d_s E\eta A_d}}p_1 \tag{16}$$

Substituting this into Eq. (15) and still using that:

$$j = -\frac{P_s}{d_s}\frac{1}{1 + \frac{P_s}{d_s E\eta A_d}}p_1 \tag{17}$$

And through the uncoated polymer substrate, the flux of the gas molecules can be easily calculated, which is:

$$j_s = -\frac{P_s}{d_s}p_1 \tag{18}$$

The gas transmission rate ratio then is:

$$TR_{ratio} = \frac{j}{j_s} = \frac{1}{1 + \frac{P_s}{d_s E\eta A_d}} \tag{19}$$

Considering that the pinhole density is equal to the reciprocal square of the distance of the pinholes (evenly distributed), $\eta = 1/L^2$, we obtain how the gas transmission rate ratio depends on the distance of the pinholes:

$$TR_{ratio} = \frac{1}{1 + \frac{P_s}{d_s E}\frac{L^2}{A_d}} \tag{20}$$

By fitting the data points for the pinholes by Eq. (20), we get 0,05 for P_s/E, which is just equal to the half edge length of the pinhole ($r/2$), or we may say to the radius of the pinhole (r_0). To check if this is just a coincidence, we can try to determine how E depends on the parameters of our system.

There is a class of steady-state diffusion problems which is characterized by diffusional flow from a region, say one side of a membrane, through a cylinder (or cylinders), called pore(s), into a large surrounding region, say on the other side of the membrane, called the reservoir. Gray, Mathews and MacRobert have given an exact solution for a zero thick pore [117]. Other papers have focused on the problem of steady-state diffusion through pores with finite thickness [118–121].

They deduced that the current of a solute in a fluid through an infinitely thin pore with a radius of r_0 is $4Dr_0\Delta\rho$, so the flux is this divided by $A_d = (2r_0)^2$:

$$j_d = \frac{D}{r_0}\Delta\rho \tag{21}$$

where D is the diffusion coefficient of the solute in the fluid and $\Delta\rho$ is the concentration difference on the two sides of the hole. In the case of diffusion of vapor through a membrane, the surface concentrations may not be known but only the vapor pressure. If the diffusion coefficient is constant, and if the sorption isotherm is linear, that is, there is a linear relationship between the external vapor pressure and the corresponding equilibrium concentration within the membrane, $\rho = Sp$ (see Eq. (2)), we may write:

$$j_d = \frac{D_s S}{r_0}\Delta p, \tag{22}$$

where D_s denotes the diffusion coefficient of the gas molecules in the polymer substrate. And the D_sS product is just the P_s permeability coefficient of the substrate [100]. Comparing Eq. (22) to Eq. (12), we obtain that $E = P_s/r_0$. Substituting this into Eq. (20), we get:

$$TR_{ratio} = \frac{1}{1 + \frac{r_0}{d_s}\frac{L^2}{A_d}} \tag{23}$$

At first sight, this seems very different from Muller and Weisser's

equation, Eq. (4). However, using that $\Theta = A_d/L^2$, this equation can also be written in the following form:

$$TR_{ratio} = \frac{\Theta}{\frac{r_0}{d_s} + \Theta} \tag{24}$$

which suggests that the two formulas are identical if $1 - \exp\left(-0,432\frac{2r_0}{d_s}\right) = \frac{r_0}{d_s}$. And indeed, considering that $r_0 \ll d_s$, $1 - \exp\left(-0,432\frac{2r_0}{d_s}\right) \approx 0,432\frac{2r_0}{d_s} \approx \frac{r_0}{d_s}$, that Muller and Weisser's empirical equation obtained from numerical simulation data and Eq. (24) are equivalent.

Note that Fabrikant also investigated the problem of impermeable membrane perforated by a set of arbitrarily located holes and considered the flow through the pores [120,121]. He showed that the interaction decreases the flux up to 25% for two closely located pores. This means that E must be L-dependent, the effect of which increases towards small Ls. According to Fabrikant's calculations, for $L > 10r_0$ the reduction is less than 6%. Accordingly, Eqs. (23) and (24) must be a good estimation over the entire practically important range of L.

A similar calculation was not found in the literature for cracks. However, we can try to fit the obtained data points with a function similar to Eq. (23):

$$TR_{ratio} = \frac{1}{1 + \frac{a}{\Theta^k}} or TR_{ratio} = \frac{\Theta^k}{a + \Theta^k} \tag{25}$$

Note that $\Theta = w/L$ for parallel cracks and $\Theta = A_d/L^2$ for pinholes. This function fits perfectly to the data points as can be seen in Fig. 8. The value of k is 1,25 for both parallel and crossing cracks. The value of a is 0,033 and 0,076. The parameter a and k could be determined for a given defect geometry following a similar calculation as was done in Reference [118–121] and Eqs. (12–24). That would be quite laborious. However, Eq. (25) appears to be a generally valid equation in which parameters a and k characterize the gas permeability of the defective barrier layer/-polymer substrate system. And as was shown above, these parameters can be given for pinholes: $a = r_0/d_s$ and $k = 1$.

5.4. Gas transmission rate ratio versus defect distance – experiments

The results of the measurements on the cracked samples naturally include the contribution of pinholes. To correct this to some extent, from the measured CO_2TR values, we subtracted the pinhole contribution obtained when measuring the uncracked samples–although, the contribution is not purely additive due to interaction of the defects, i.e. the overlapping diffusion fields. However, the simulation results fit better to the corrected measurement points and can be perfectly fitted with Eq. (25), as can be seen in Fig. 10. The figure also shows the corresponding simulated points for parallel and crossing cracks.

As can be seen the simulation somewhat overestimates the measured values for lower crack density (for higher L values). Unsurprisingly, we still do not get exactly the same values from the simulation as from the measurements.

It can be clearly seen in the SEM images (Fig. 11) the cracks are not arranged in an orderly manner as in the simulation.

This, in turn, greatly influences the course of the curve according to computer simulations. The numerical simulations for arrays of pinholes performed by Toni, Baschetti, Lorenzetti, Fayet and Sarti showed that the average flux obtained for each different defectiveness is not a fixed value, but rather shows substantial variations due to the randomness of the defect distribution [103]. They also found that in the case of a random defect distribution, the gas transmission rate ratio versus defect distance curve is significantly steeper than in the case of regularly arranged defects. In the case of the fitted curve in Fig. 10, the value of k is 2,5, which is higher than the value obtained from the simulation. We believe that the value of k is related to the randoness of the defect distribution, which is consistent with the results of Toni et al. [103].

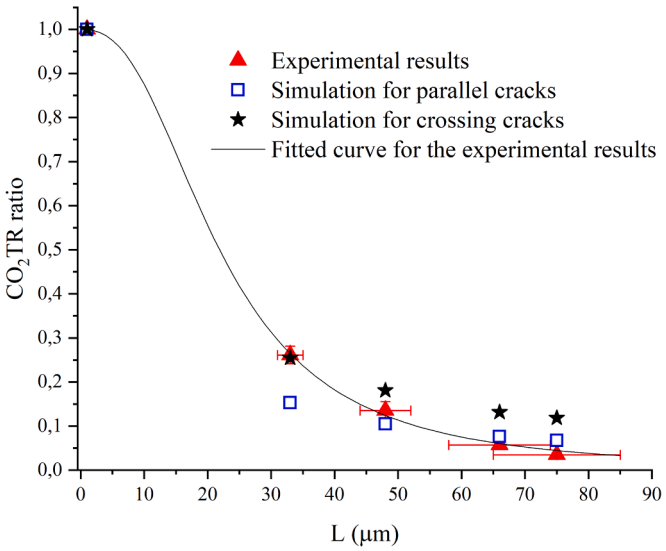

Fig. 10. Experimental results and the fitted curve described by Eq. (25). The contribution of pinholes to the total transmission data has been subtracted. Estimation by computer simulation for parallel and crossing cracks is also shown.

It should also be noted that not only the defect distance has a random distribution, but the width of the cracks also varies with the thickness of the oxide layer, and it also has a random distribution. Thus, it is quite difficult to reproduce the experimental results by computer simulation one by one. Nevertheless, the simulations provided a good predictor of the range in which the gas permeability values could be expected for samples with different layer thicknesses. They also help to understand how deviations from an ideally ordered defect distribution change the gas permeability of the oxide/substrate system.

It is important to note that the differences observed between the individual measurements are certainly not only due to measurement uncertainty, but to the interaction of the defects, which has a significant effect on the permeability of each defect.

6. Conclusions

Atomic layer deposited ultra-barrier films with low water vapor and gas permeability have been investigated recently for industrial applications. Aluminum-oxide (Al_2O_3) thin layers are widely used on flexible polymer surfaces to enhance diffusion barrier performance. However, there are mechanical limitations that could restrict the encapsulation utility of these films. Very few studies have explored the mechanical properties of layers prepared by plasma enhanced atomic layer deposition, even less papers are available about how this could influence the barrier behavior. In this investigation, we integrated the effect of „intrinsic" defects in the layers, such as pinholes, and the influence of in situ cracking of thin oxide layers based on experimental data into computer simulations to show how these complex defect structures can alter the barrier usefulness.

Our experimental results for the uncracked films containing pinholes are in very good agreement with the value obtained from previous datasets [113]. Furthermore, after the in situ cracking procedure, the results of the analysis of the electron microscopic images of our defected layers revealed that crack density is inversely proportional to the square root of the Al_2O_3 layer thickness, so the proportionality found by Jen et al. is also met in our case [24]. In addition, we showed that the CO_2 permeation rate across the defected layers decrease in exponential manner as the layer thickness increases: quadrupling the film thickness reduced it by a tenth. This implies that under the same mechanical load

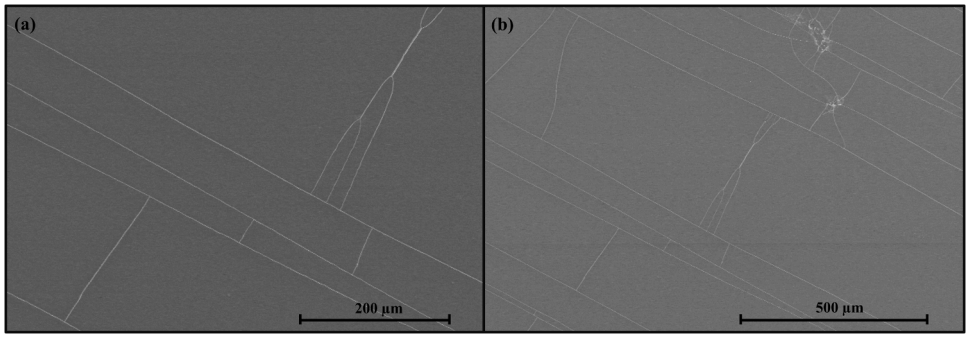

Fig. 11. SEM image of crack network for a 100 nm thick Al_2O_3 layer with 200x (a) and with 100x magnification (b). The cracks are randomly arranged, their distance is not equal.

there is a threshold value in the coating thickness, where the barrier efficiency and cost ratio are the most beneficial.

To explore how crossing cracks affect the gas transmission rate ratio, we also simulated crack networks with a rectangular lattice geometry. As expected, the gas transmission rate ratio in this case is significantly higher than in the case of parallel cracks only. Note that although the surface area of the cracks is two times larger in the case of crossing cracks than in the case of parallel cracks, the ratio of the gas transmission rate follows a different trend. When L is small, the ratio of the two cases i.e. two datasets is close to one. With increasing defect distances this proportion also increases and approaches two-fold. This is consistent with the image that the more the diffusion fields overlap, the more the overall permeating flux is reduced.

Taking into consideration the effusion and diffusion processes we constructed an analytical model to describe how the gas transmission rate ratio can depend on the defect (pinhole or crack) distance. Using this theoretical calculation, we established an equation, which appears to be generally valid for several practically important cases. In this correlation, the parameters a and k characterize the gas permeability of the defective barrier layer/polymer substrate systems. The parameter a is related to the thickness of the substrate and the geometry of the defects in the coating layer, whereas we believe that the value of k is related to the randomness of the defect distribution, which also plays an important role in the most realistic approaches. It should also be noted that not only the formation of pinholes and cracks vary randomly from sample to sample, but the defect distances, the width of the cracks also vary with the thickness of the oxide layer, and all of these have a random distribution. Thus, it is quite difficult to reproduce the experimental results one by one. Nevertheless, the simulations provided a good predictor of the range in which the gas permeability values could be expected for samples with different layer thicknesses. They also help to understand how deviations from an ideally ordered defect distribution change the gas permeability of the oxide/substrate system.

This introduced measurement setup, experimental and theoretical work fills a gap in the literature and may open further perspectives in understanding defective barrier layers and their behaviors under mechanical loading.

CRediT authorship contribution statement

Réka Lilla Kovács: Conceptualization, Methodology, Formal analysis, Investigation, Data curation, Validation, Writing – original draft. **Szilvia Gyöngyösi:** Investigation, Methodology. **Gábor Langer:** Methodology, Writing – review & editing. **Eszter Baradács:** Investigation, Formal analysis, Data curation. **Lajos Daróczi:** Resources. **Péter Barkóczy:** Resources. **Zoltán Erdélyi:** Conceptualization, Methodology, Supervision, Formal analysis, Validation, Investigation, Writing – original draft, Funding acquisition.

Declaration of Competing Interest

The authors declare that they have no known competing financial interests or personal relationships that could have appeared to influence the work reported in this paper.

Acknowledgments

The work is supported by the European Union and the European Regional Development Fund (GINOP-2.3.2–15–2016–00041). Project no. TKP2020-NKA-04 has been implemented with the support provided from the National Research, Development and Innovation Fund of Hungary, financed under the 2020–4.1.1-TKP2020 funding scheme.

Data Availability

The data that support the findings of this study are available within the article. Additional data that support the findings of this study are available from the corresponding author upon reasonable request.

References

[1] S. Alavi, S. Thomas, K.P. Sandeep, N. Kalarikkal, J. Varghese, S. Yaragalla, Polymers For Packaging Applications, CRC Press, Boca Raton, 2014.
[2] J. González, A. Ferrer, R. Oria, M.L. Salvador, Determination of O_2 and CO_2 transmission rates through microperforated films for modified atmosphere packaging of fresh fruits and vegetables, J. Food Eng. 86 (2008) 194–201, https://doi.org/10.1016/j.jfoodeng.2007.09.023.
[3] X. Zhang, H. Wang, N. Li, M. Li, X. Xu, High CO_2-modified atmosphere packaging for extension of shelf-life of chilled yellow-feather broiler meat: a special breed in Asia, Food Sci. Technol. 64 (2015) 1123–1129, https://doi.org/10.1016/j.lwt.2015.07.039.
[4] I.J. Church, A.L. Parsons, Modified atmosphere packaging technology: a review, Sci. Food Agric. 67 (1995) 143–152, https://doi.org/10.1002/jsfa.2740670202.
[5] R. Simpson, C. Acevedo, S. Almonacid, Mass transfer of CO_2 in MAP systems: advances for non-respiring foods, J. Food Eng. 92 (2009) 233–239, https://doi.org/10.1016/j.jfoodeng.2008.10.035.
[6] S.D.F. Mihindukulasuriya, L.-.T. Lim, Nanotechnology development in food packaging: a review, Trends Food Sci. Technol. 40 (2014) 149–167, https://doi.org/10.1016/j.tifs.2014.09.009.
[7] M.D. Groner, F.H. Fabreguette, J.W. Elam, S.M. George, Low-temperature Al_2O_3 atomic layer deposition, Chem. Mater. 16 (2004) 639–645, https://doi.org/10.1021/cm0304546.
[8] H. Chatham, Oxygen diffusion barrier properties of transparent oxide coatings on polymeric substrates, Surf. Coat. Technol. 78 (1996) 1–9, https://doi.org/10.1016/0257-8972(95)02420-4.
[9] K. Lahtinen, P. Johansson, T. Kääriäinen, D.C. Cameron, Adhesion of extrusion-coated polymer sealing layers to a fiber-based packaging material with an atomic layer deposited aluminum oxide surface coating, Polym. Eng. Sci. 52 (2012) 1985–1990, https://doi.org/10.1002/pen.23148.
[10] T.O. Kääriäinen, P. Maydannik, D.C. Cameron, K. Lahtinen, P. Johansson, J. Kuusipalo, Atomic layer deposition on polymer based flexible packaging materials: growth characteristics and diffusion barrier properties, Thin Solid Films 519 (2011) 3146–3154, https://doi.org/10.1016/j.tsf.2010.12.171.
[11] J. Fahlteich, M. Fahland, W. Schönberger, N. Schiller, Permeation barrier properties of thin oxide films on flexible polymer substrates, Thin Solid Films 517 (2009) 3075–3080, https://doi.org/10.1016/j.tsf.2008.11.089.
[12] S.M. George, Atomic layer deposition: an overview, Chem. Rev. 110 (2010) 111–131, https://doi.org/10.1021/cr900056b.

[13] H. Profijt, S.E. Potts, M.C.M. Sanden, W.M.M. Kessels, Plasma-assisted atomic layer deposition: basics, opportunities, and challenges, J. Vac. Sci. Technol. 29 (2011), 050801, https://doi.org/10.1116/1.3609974.

[14] L. Hoffmann, D. Theirich, T. Hasselmann, A. Räupke, D. Schlamm, T. Riedl, Gas permeation barriers deposited by atmospheric pressure plasma enhanced atomic layer deposition, J. Vac. Sci. Technol. 34 (2015) 01A114, https://doi.org/10.1116/1.4935337.

[15] S.E. Potts, W. Keuning, E. Langereis, G. Dingemans, M.C.M. Sanden, W.M. M. Kessels, Low temperature plasma-enhanced atomic layer deposition of metal oxide thin films, J. Electrochem. Soc. 157 (2010) P66–P74, https://doi.org/10.1149/1.3428705.

[16] H.C. Guo, E. Ye, Z. Li, M.-.Y. Han, X.J. Loh, Recent progress of atomic layer deposition on polymeric materials, Mater. Sci. Eng. C. 70 (2017) 1182–1191, https://doi.org/10.1016/j.msec.2016.01.093.

[17] H. Kim, Characteristics and applications of plasma enhanced-atomic layer deposition, Thin Solid Films 519 (2011) 6639–6644, https://doi.org/10.1016/j.tsf.2011.01.404.

[18] H. Kim, S.S. Kim, Aluminum oxide barrier coating on polyethersulfone substrate by atomic layer deposition for barrier property enhancement, Thin Solid Films 520 (2011) 481–485, https://doi.org/10.1016/j.tsf.2011.06.096.

[19] J.-.S. Park, H. Chae, H. Chung, S. Lee, Thin film encapsulation for flexible AM-OLED: a review, Semicond. Sci. Technol. 26 (2011), 034001, https://doi.org/10.1088/0268-1242/26/3/034001.

[20] S.-.H. Park, J. Oh, C.-.S. Hwang, J.-.I. Lee, Y.S. Yang, H. Chu, K.-.Y. Kang, Ultra-thin film encapsulation of OLED on plastic substrate, J. Inf. Disp. 27 (2005) 545–550, https://doi.org/10.1080/15980316.2004.9651953.

[21] N. Kim, S. Graham, Development of highly flexible and ultra-low permeation rate thin-film barrier structure for organic electronics, Thin Solid Films 547 (2013) 57–62, https://doi.org/10.1016/j.tsf.2013.05.007.

[22] A.P. Roberts, B.M. Henry, A.P. Sutton, C.R.M. Grovenor, G.A.D. Briggs, T. Miyamoto, M. Kano, Y. Tsukahara, M. Yanaka, Gas permeation in silicon-oxide/polymer (SiOx/PET) barrier films: role of the oxide lattice, nano-defects and macro-defects, J. Membr. Sci. 208 (2002) 75–88, https://doi.org/10.1016/S0376-7388(02)00178-3.

[23] J. Sheng, K.-.L. Han, T. Hong, W.-.H. Choi, J.-.S. Park, Review of recent progresses on flexible oxide semiconductor thin film transistors based on atomic layer deposition processes, J. Semicond. 39 (2018), 011008, https://doi.org/10.1088/1674-4926/39/1/011008.

[24] S.-.H. Jen, J.A. Bertrand, S.M. George, Critical tensile and compressive strains for cracking of Al_2O_3 films grown by atomic layer deposition, J. Appl. Phys. 109 (2011), 084305, https://doi.org/10.1063/1.3567912.

[25] Y. Zhang, R. Yang, S.M. George, Y.-.C. Lee, In-situ inspection of cracking in atomic-layer-deposited barrier films on surface and in buried structures, Thin Solid Films 520 (2011) 251–257, https://doi.org/10.1016/j.tsf.2011.07.056.

[26] A. Bulusu, H. Behm, F. Sadeghi-Tohidi, H. Bahre, E. Baumert, D. Samet, C. Hopmann, J. Winter, O. Pierron, S. Graham, The mechanical reliability of flexible ALD barrier films, SID Symp. Dig. Tech. Pap. 44 (2013) 361–364, https://doi.org/10.1002/j.2168-0159.2013.tb06221.x.

[27] Y. Leterrier, Durability of nanosized oxygen-barrier coatings on polymers, Prog. Mater. Sci. 48 (2003) 1–55, https://doi.org/10.1016/S0079-6425(02)00002-6.

[28] M. Hanika, H.-.C. Langowski, U. Moosheimer, W. Peukert, Inorganic layers on polymeric films – influence of defects and morphology on barrier properties, Chem. Eng. Technol. 26 (2003) 605–614, https://doi.org/10.1002/ceat.200390093.

[29] G. Rossi, M. Nulman, Effect of local flaws in polymeric permeation reducing barriers, J. Appl. Phys. 74 (1993) 5471, https://doi.org/10.1063/1.354227.

[30] A.S. da Silva Sobrinho, G. Czeremuszkin, M. Latrèche, M.R. Wertheimer, Defect-permeation correlation for Ultrathin transparent barrier coatings on polymers, J. Vac. Sci. Technol. 18 (2000) 149–157, https://doi.org/10.1116/1.582156.

[31] K. Lahtinen, P. Maydannik, P. Johansson, T. Kääriäinen, D.C. Cameron, J. Kuusipalo, Utilisation of continuous atomic layer deposition process for barrier enhancement of extrusion-coated paper, Surf. Coat. Technol. 205 (2011) 3916–3922, https://doi.org/10.1016/j.surfcoat.2011.02.009.

[32] E.K. Baumert, O.N. Pierron, Fatigue properties of atomic-layer-deposited alumina ultra-barriers and their implications for the reliability of flexible organic electronics, Appl. Phys. Lett. 101 (2012), 251901, https://doi.org/10.1063/1.4772471.

[33] K. Lahtinen, J. Lahti, P. Johansson, T. Seppänen, D.C. Cameron, Influence of substrate contamination, web handling, and pretreatments on the barrier performance of aluminum oxide atomic layer-deposited BOPP film, J. Coat. Technol. Res. 11 (2014) 775–784, https://doi.org/10.1007/s11998-014-9584-9.

[34] A. Behrendt, J. Meyer, P. Weijer, T. Gahlmann, R. Heiderhoff, T. Riedl, Stress management in thin-film gas-permeation barriers, ACS Appl. Mater. Interfaces. 8 (2016) 4056–4061, https://doi.org/10.1021/acsami.5b11499.

[35] S. Mani, T.M. Sai, Mechanism of controlled crack formation in thin-film dielectrics, Appl. Phys. Lett. 86 (2005), 201903, https://doi.org/10.1063/1.1927267.

[36] S.H. Mirfarsi, M.J. Parnian, S. Rowshanzamir, Self-humidifying proton exchange membranes for fuel cell applications: advances and challenges, Processes 8 (2020) 1069, https://doi.org/10.3390/pr8091069.

[37] C.H. Park, S.Y. Lee, D.S. Hwang, D.W. Shin, D.H. Cho, K.H. Lee, T.-.W. Kim, T.-.W. Kim, M. Lee, D.-.S. Kim, C.M. Doherty, A.W. Thornton, A.J. Hill, M.D. Guiver, J.M. Lee, Nanocrack-regulated self-humidifying membranes, Nature 532 (2016) 480–483, https://doi.org/10.1038/nature17634.

[38] G.-.J. Choi, S. Kim, S.-.J. Won, H. Kim, C. Hwang, Plasma-enhanced atomic layer deposition of TiO_2 and Al-Doped TiO_2 films using N_2O and O_2 reactants, J. Electrochem. Soc. 156 (2009) G138–G143, https://doi.org/10.1149/1.3169516.

[39] D. Bootkul, P. Jitsopakul, S. Intarasiri, D. Boonyawan, Qualifying ultrathin alumina film prepared by plasma-enhance atomic layer deposition under low temperature operation, Thin Solid Films 640 (2017) 116–122, https://doi.org/10.1016/j.tsf.2017.09.008.

[40] Y. Lee, S. Seo, I.-.K. Oh, S. Lee, H. Kim, Effects of O_2 plasma treatment on moisture barrier properties of SiO_2 grown by plasma-enhanced atomic layer deposition, Ceram. Int. 45 (2019) 17662–17668, https://doi.org/10.1016/j.ceramint.2019.05.332.

[41] J.W. Chiappim, G. Testoni, A. Doria, R. Pessoa, M. Fraga, N. Galvão, K. Grigorov, L. Vieira, H. Maciel, Relationships among growth mechanism, structure and morphology of PEALD TiO_2 films: the influence of O_2 plasma power, precursor chemistry and plasma exposure mode, Nanotechnology 27 (2016), 305701, https://doi.org/10.1088/0957-4484/27/30/305701.

[42] K.H. Yoon, H. Kim, Y.-.E. Lee, N.K. Shrestha, M. Sung, UV-enhanced atomic layer deposition of Al_2O_3 thin films at low temperature for gas-diffusion barriers, RSC Adv. 7 (2017) 5601–5609, https://doi.org/10.1039/C6RA27759D.

[43] S.-.W. Seo, E. Jung, C. Lim, H. Chae, S.M. Cho, Moisture permeation through Ultrathin TiO_2 films grown by atomic layer deposition, Appl. Phys. Express. 5 (2012), 035701, https://doi.org/10.1143/APEX.5.035701.

[44] W. Kim, M.-.G. Ko, T.-.S. Kim, S.-.K. Park, Y.-.K. Moon, S. Lee, J.-.G. Park, J.-.W. Park, Titanium dioxide thin films deposited by plasma enhanced atomic layer deposition for OLED passivation, J. Nanosci. Nanotechnol. 8 (2008) 4726–4729, https://doi.org/10.1166/jnn.2008.IC48.

[45] D.-.Y. Su, Y.-.H. Kuo, M. Tseng, F.-.Y. Tsai, Effects of surface pretreatment and deposition conditions on the gas permeation properties and flexibility of Al_2O_3 films on polymer substrates by atomic layer deposition, J. Coat. Technol. Res. 16 (2019) 1751–1756, https://doi.org/10.1007/s11998-019-00238-x.

[46] J.G. Lee, H. Kim, S.S. Kim, Enhancement of barrier properties of aluminum oxide layer by optimization of plasma-enhanced atomic layer deposition process, Thin Solid Films 534 (2013) 515–519, https://doi.org/10.1016/j.tsf.2013.02.125.

[47] O. Ylivaara, L. Kilpi, X. Liu, S. Sintonen, S. Ali, M. Laitinen, J. Julin, E. Haimi, T. Sajavaara, H. Lipsanen, S.-.P. Hannula, H. Ronkainen, R. Puurunen, Aluminum oxide/titanium dioxide nanolaminates grown by atomic layer deposition: growth and mechanical properties, J. Vac. Sci. Technol. 35 (2016) 01B105, https://doi.org/10.1116/1.4966198.

[48] J.G. Lee, H.G. Kim, S.S. Kim, Defect-sealing of Al_2O_3/ZrO_2 multilayer for barrier coating by plasma-enhanced atomic layer deposition process, Thin Solid Films 577 (2015) 143–148, https://doi.org/10.1016/j.tsf.2015.01.040.

[49] J. Meyer, P. Görrn, F. Bertram, S. Hamwi, T. Winkler, H.-.H. Johannes, T. Weimann, P. Hinze, T. Riedl, W. Kowalsky, Al_2O_3/ZrO_2 nanolaminates as ultrahigh gas-diffusion barriers—a strategy for reliable encapsulation of organic electronics, Adv. Mater. 21 (2009) 1845–1849, https://doi.org/10.1002/adma.200803440.

[50] A. Dameron, S. Davidson, B. Burton, P. Carcia, R. McLean, S.M. George, Gas diffusion barriers on polymers using multilayers fabricated by Al_2O_3 and rapid SiO_2 atomic layer deposition, J. Phys. Chem. C. 112 (2008) 4573–4580, 10.1021/jp076866±.

[51] L. Kim, Y. Jeong, T. Kyu, S. Park, J. Jang, S. Nam, J. Jang, S. Kim, C. Park, Optimization of Al_2O_3/TiO_2 nanolaminate thin films prepared with different oxide ratios, for use in organic light-emitting diode encapsulation, via plasma-enhanced atomic layer deposition, Phys. Chem. Chem. Phys. 18 (2015) 1042–1049, https://doi.org/10.1039/C5CP06713H.

[52] L. Kim, K. Kim, S. Park, Y. Jeong, H. Kim, D. Chung, S. Kim, C. Park, Al_2O_3/TiO_2 nano-laminate thin film encapsulation for organic thin film transistors via plasma-enhanced atomic layer deposition, ACS Appl. Mater. Interfaces. 6 (2014) 6731–6738, https://doi.org/10.1021/am500458d.

[53] T. Ahmadzada, D.R. McKenzie, N.L. James, Y. Yin, Q. Li, Atomic layer deposition of Al_2O_3 and Al_2O_3/TiO_2 barrier coatings to reduce the water vapour permeability of polyetheretherketone, Thin Solid Films 591 (2015) 131–136, https://doi.org/10.1016/j.tsf.2015.08.038.

[54] P.F. Carcia, R.S. McLean, M.D. Groner, A.A. Dameron, S.M. George, Gas diffusion ultrabarriers on polymer substrates using Al_2O_3 atomic layer deposition and SiN plasma-enhanced chemical vapor deposition, J. Appl. Phys. 106 (2009), 023533, https://doi.org/10.1063/1.3159639.

[55] A. Bulusu, A. Singh, C. Wang, A. Dindar, C. Fuentes-Hernandez, H. Kim, D. Cullen, B. Kippelen, S. Graham, Engineering the mechanical properties of ultrabarrier films grown by atomic layer deposition for the encapsulation of printed electronics, J. Appl. Phys. 118 (2015), 085501, https://doi.org/10.1063/1.4928855.

[56] P. Carcia, R.R. McLean, Z. Li, M. Reilly, W. Marshall, Permeability and corrosion in ZrO_2/Al_2O_3 nanolaminate and Al_2O_3 thin films grown by atomic layer deposition on polymers, J. Vac. Sci. Technol. 30 (2012), 041515, https://doi.org/10.1116/1.4729447.

[57] D.-.S. Han, D.-.K. Choi, J.-.W. Park, Al_2O_3/TiO_2 multilayer thin films grown by plasma enhanced atomic layer deposition for organic light-emitting diode passivation, Thin Solid Films 552 (2014) 155–158, https://doi.org/10.1016/j.tsf.2013.12.003.

[58] N. Kim, W.J. Potscavage, A. Sundaramoothi, C. Henderson, S.Graham B.Kippelen, A correlation study between barrier film performance and shelf lifetime of encapsulated organic solar cells, Sol. Energy Mater. Sol. Cells. 101 (2012) 140–146, https://doi.org/10.1016/j.solmat.2012.02.002.

[59] M. Park, S. Oh, H. Kim, D. Jung, D. Choi, J.-.S. Park, Gas diffusion barrier characteristics of Al_2O_3/alucone films formed using trimethylaluminum, water

and ethylene glycol for organic light emitting diode encapsulation, Thin Solid Films 546 (2013) 153–156, https://doi.org/10.1016/j.tsf.2013.05.017.
[60] W. Xiao, D. Hui, C. Zheng, Y. Duan, Y. Qiang, C. Ping, C. Xiang, Z. Yi, A flexible transparent gas barrier film employing the method of mixing ALD/MLD-grown Al_2O_3 and alucone layers, Nanoscale Res. Lett. 10 (2015) 130, https://doi.org/10.1186/s11671-015-0838-y.
[61] R. Long, M.L. Dunn, Channel cracks in atomic-layer and molecular-layer deposited multilayer thin film coatings, J. Appl. Phys. 115 (2014), 233514, https://doi.org/10.1063/1.4884438.
[62] M.M. ur Rehman, K.T. Kim, K.H. Na, K.H. Choi, Atmospheric deposition process for enhanced hybrid organic–inorganic multilayer barrier thin films for surface protection, Appl. Surf. Sci. 422 (2017) 273–282, https://doi.org/10.1016/j.apsusc.2017.05.261.
[63] S.-.W. Seo, E. Jung, H. Chae, S.J. Seo, H.K. Chung, S.M. Cho, Bending properties of organic–inorganic multilayer moisture barriers, Thin Solid Films 550 (2014) 742–746, https://doi.org/10.1016/j.tsf.2013.11.072.
[64] E.G. Jeong, Y.C. Han, H.-.G. Im, B.-.S. Bae, K.C. Choi, Highly reliable hybrid nano-stratified moisture barrier for encapsulating flexible OLEDs, Org. Electron. 33 (2016) 150–155, https://doi.org/10.1016/j.orgel.2016.03.015.
[65] P. Johansson, H. Teisala, K. Lahtinen, J. Kuusipalo, Protecting an atomic layer deposited aluminum oxide barrier coating on a flexible polymer substrate, Thin Solid Films 621 (2017) 151–155, https://doi.org/10.1016/j.tsf.2016.11.034.
[66] D. Miller, R. Foster, Y. Zhang, S.-.H. Jen, J. Bertrand, Z. Lu, D. Seghete, J. Opatchen, R. Yang, Y.-.C. Lee, S.M. George, M. Dunn, The mechanical robustness of atomic-layer- and molecular-layer-deposited coatings on polymer substrates, J. Appl. Phys. 105 (2009), 093527, https://doi.org/10.1063/1.3124642.
[67] Y. Han, E. Kim, W. Kim, H.-.G. Im, B.-.S. Bae, K. Choi, A flexible moisture barrier comprised of a SiO_2-embedded organic–inorganic hybrid nanocomposite and Al_2O_3 for thin-film encapsulation of OLEDs, Org. Electron. 14 (2013) 1435–1440, https://doi.org/10.1016/j.orgel.2013.03.008.
[68] J. Greener, K.C. Ng, K.M. Vaeth, T.M. Smith, Moisture permeability through multilayered barrier films as applied to flexible OLED display, J. Appl. Polym. Sci. 106 (2007) 3534–3542, https://doi.org/10.1002/app.26863.
[69] K.L. Jarvis, P.J. Evans, Growth of thin barrier films on flexible polymer substrates by atomic layer deposition, Thin Solid Films 624 (2017) 111–135, https://doi.org/10.1016/j.tsf.2016.12.055.
[70] C. Charton, N. Schiller, M. Fahland, A. Holländer, A. Wedel, K. Noller, Development of high barrier films on flexible polymer substrates, Thin Solid Films 502 (2006) 99–103, https://doi.org/10.1016/j.tsf.2005.07.253.
[71] T. Hirvikorpi, M. Vähä-Nissi, J. Nikkola, A. Harlin, M. Karppinen, Thin Al_2O_3 barrier coatings onto temperature-sensitive packaging materials by atomic layer deposition, Surf. Coat. Technol. 205 (2011) 5088–5092, https://doi.org/10.1016/j.surfcoat.2011.05.017.
[72] S. Schubert, H. Klumbies, L. Müller-Meskamp, K. Leo, Electrical calcium test for moisture barrier evaluation for organic devices, Rev. Sci. Instrum. 82 (2011), 094101, https://doi.org/10.1063/1.3633956.
[73] A. Suzuki, H. Takahagi, A. Uehigashi, S. Hara, Development of reliable technique for evaluating the properties of water vapor barriers, AIP Adv 5 (2015), 117204, https://doi.org/10.1063/1.4935341.
[74] X.-.D. Zhang, J. Lewis, C. Parker, J. Glass, S. Wolter, Measurement of reactive and condensable gas permeation using a mass spectrometer, J. Vac. Sci. Technol. 26 (2008) 1128–1137, https://doi.org/10.1116/1.2952453.
[75] P. Hülsmann, D. Philipp, M. Köhl, Measuring temperature-dependent water vapor and gas permeation through high barrier films, Rev. Sci. Instrum. 80 (2009), 113901, https://doi.org/10.1063/1.3250866.
[76] X.Q. Nguyen, Z. Brož, F. Vašák, Q.T. Nguyen, Manometric techniques for determination of gas transport parameters in membranes. Application to the study of dense and asymmetric poly(vinyltrimethylsilane) membranes, J. Membr. Sci. 91 (1994) 65–76, https://doi.org/10.1016/0376-7388(94)00019-0.
[77] H. Yoshida, T. Ebina, K. Arai, T. Kobata, R. Ishii, T. Aizawa, A. Suzuki, Development of water vapor transmission rate measuring device using a quadrupole mass spectrometer and standard gas barrier films down to the 10^{-6} g m^{-2} day^{-1} level, Rev. Sci. Instrum. 88 (2017), 043301, https://doi.org/10.1063/1.4980074.
[78] J.C. Tou, D.C. Rulf, P.T. DeLassus, Mass spectrometric system for the measurement of aroma/flavor permeation rates across polymer films, Anal. Chem. 62 (1990) 592–597, https://doi.org/10.1021/ac00205a010.
[79] J. Lewis, Material challenge for flexible organic devices, Mater. Today. 9 (2006) 38–45, https://doi.org/10.1016/S1369-7021(06)71446-8.
[80] G. Rochat, P. Fayet, Characterization of mechanical properties of ultra-thin oxide coatings on polymers by uniaxial fragmentation tests, J. Adhes. Sci. Tech. 26 (2012) 1–12, https://doi.org/10.1163/156856111X599517.
[81] M.V.T. da Costa, J. Bolinsson, R.C. Neagu, P. Fayet, E.K. Gamstedt, Experimental assessment of micromechanical models for fragmentation analysis of thin metal oxide coatings on polymer films under uniaxial tensile deformation, Surf. Coat. Technol. 370 (2019) 374–383, https://doi.org/10.1016/j.surfcoat.2019.03.035.
[82] L. Marras, O. Sbaizero, The fragmentation test applied to adhesion measurements and microstructural characterization in plasma pre-treated metallized plastic webs, Packag. Technol. Sci. 22 (2009) 293–302, https://doi.org/10.1002/pts.854.
[83] M. Ruoho, J.-.P. Niemelä, C. Guerra, N. Tarasiuk, G. Robertson, A. Taylor, X. Maeder, C. Kapusta, J. Michler, I. Utke, Thin-film engineering of mechanical fragmentation properties of atomic-layer-deposited metal oxides, Nanomaterials 10 (2020) 558, https://doi.org/10.3390/nano10030558.
[84] M.V.T. da Costa, J. Bolinsson, P. Fayet, E.K. Gamstedt, Transverse ridge cracking in tensile fragmentation tests of thin brittle coatings on polymer substrates, Surf. Coat. Technol. 382 (2020), 125025, https://doi.org/10.1016/j.surfcoat.2019.125025.
[85] Z. Tang, L. Ye, Characterisation of mechanical properties of thin polymer films using a bi-axial tension based on blow-up test, Plast. Rubber Compos. 32 (2003) 459–465, https://doi.org/10.1179/146580103225004379.
[86] M. Small, W.D. Nix, Analysis of the accuracy of the bulge test in determining the mechanical properties of thin films, J. Mater. Res. 7 (1992) 1553–1563, https://doi.org/10.1557/JMR.1992.1553.
[87] J. Andersons, Y. Leterrier, I. Fescenko, Analysis of the initial fragmentation stage of oxide coatings on polymer substrates under biaxial tension, Thin Solid Films 434 (2003) 203–215, https://doi.org/10.1016/S0040-6090(03)00482-6.
[88] P.-.I. Hsu, M. Huang, H. Gleskova, Z. Xi, Z. Suo, S. Wagner, J. Sturm, Effects of mechanical strain on TFTs on spherical domes, electron devices, IEEE Trans. Electron. Devices 51 (2004) 371–377, https://doi.org/10.1109/TED.2003.822873.
[89] M. Berdova, O. Ylivaara, V. Rontu, P. Torma, R. Puurunen, S. Franssila, Fracture properties of atomic layer deposited aluminum oxide free-standing membranes, J. Vac. Sci. Technol. 33 (2015) 01A106, https://doi.org/10.1116/1.4893769.
[90] M. Berdova, T. Ylitalo, I. Kassamakov, J. Heino, P.T. Törmä, L. Kilpi, H. Ronkainen, J. Koskinen, E. Hæggström, S. Franssila, Mechanical assessment of suspended ALD thin films by bulge and shaft-loading techniques, Acta Mater. 66 (2014) 370–377, https://doi.org/10.1016/j.actamat.2013.11.024.
[91] D. Xu, K. Liechti, Bulge testing transparent thin films with moir deflectometry, Exp. Mech. 50 (2009) 217–225, https://doi.org/10.1007/s11340-009-9291-0.
[92] S. Grego, J. Lewis, E. Vick, D. Temple, Development and evaluation of bending-testing techniques for flexible-display applications, J. Soc. Inf. Disp. 13 (2005) 575–581, https://doi.org/10.1889/1.2001215.
[93] M. Yanaka, B.M. Henry, A.P. Roberts, C.R.M. Grovenor, G.A.D. Briggs, A. P. Sutton, T. Miyamoto, Y. Tsukahara, N. Takeda, R.J. Chater, How cracks in SiOx-coated polyester films affect gas permeation, Thin Solid Films 397 (2001) 176–185, https://doi.org/10.1016/S0040-6090(01)01473-0.
[94] C.P. Barker, K.-.H. Kochem, K.M. Revell, R.S.A. Kelly, J.P.S. Badyal, Atomic force microscopy and permeability study of stretching-induced gas barrier loss of AlOx layers, Thin Solid Films 259 (1995) 46–52, https://doi.org/10.1016/0040-6090(95)80054-9.
[95] T. Futatsugi, S. Ogawa, M. Takemoto, M. Yanaka, Y. Tsukahara, Integrity evaluation of SiOx film on polyethylene terapthalate by AE characterization and laser microscopy, NDT E Int. 29 (1996) 307–316, https://doi.org/10.1016/S0963-8695(96)00034-5.
[96] Y. Zhang, Y.-.Z. Zhang, D. Miller, J. Bertrand, S.-.H. Jen, R. Yang, M. Dunn, S. M. George, Y.C. Lee, Fluorescent tags to visualize defects in Al_2O_3 thin films grown using atomic layer deposition, Thin Solid Films 517 (2009) 6794–6797, https://doi.org/10.1016/j.tsf.2009.05.037.
[97] S.-.H. Jen, B.H. Lee, S.M. George, R.S. McLean, P.F. Carcia, Critical tensile strain and water vapor transmission rate for nanolaminate films grown using Al_2O_3 atomic layer deposition and alucone molecular layer deposition, Appl. Phys. Lett. 101 (2012), 234103, https://doi.org/10.1063/1.4766731.
[98] K. Kim, O. Pierron, S. Graham, Atomic layer deposited Al_2O_3 capping layer effect on environmentally assisted cracking in SiNx barrier films, J. Appl. Phys. 125 (2019), 045301, https://doi.org/10.1063/1.5061780.
[99] S.-.W. Seo, E. Jung, H. Chae, S.J. Seo, H.K. Chung, S.M. Cho, Bending properties of organic-inorganic multilayer moisture barriers, Thin Solid Films 550 (2014) 742–746, https://doi.org/10.1016/j.tsf.2013.11.072.
[100] J. Crank, The Mathematics of Diffusion, Clarendon Press, New York, 1979.
[101] K. Mueller, H. Weisser, Numerical simulation of permeation through vacuum-coated laminate films, Packag. Technol. Sci. 15 (2002) 29–36, https://doi.org/10.1002/pts.563.
[102] A. Grüniger, P.R. von Rohr, Influence of defects in SiOx thin films on their barrier properties, Thin Solid Films 459 (2004) 308–312, https://doi.org/10.1016/j.tsf.2003.12.146.
[103] E. Toni, M.G. Baschetti, C. Lorenzetti, P. Fayet, G.C. Sarti, Effects of random defect distributions in the barrier coating on the gas permeability of multilayer films, Surf. Coat. Technol. 302 (2016) 65–74, https://doi.org/10.1016/j.surfcoat.2016.04.071.
[104] F. Hecht, New development in FreeFem++, J. Numer. Math. 20 (2012) 251–266, https://doi.org/10.1515/jnum-2012-0013.
[105] H. Si, TetGen, a Delaunay-Based Quality Tetrahedral mesh generator, ACM Trans. Math. Softw. 41 (2015) 1–36, https://doi.org/10.1145/2629697.
[106] S. Selke, R.J. Hernandez, et al., Packaging: polymers in flexible packaging, in: K. H. Jürgen Buschow, Robert W. Cahn, Merton C. Flemings, Bernhard Ilschner, Edward J. Kramer, Subhash Mahajan, et al. (Eds.), Encyclopedia of Materials: Science and Technology, Elsevier, 2001.
[107] J. Ferguson, A.W. Weimer, S.M. George, Atomic layer deposition of Al_2O_3 films on polyethylene particles, Chem. Mater. 16 (2004) 5602–5609, https://doi.org/10.1021/cm040008y.
[108] M. Vaha-Nissi, M. Pitkänen, E. Salo, J. Sievänen, M. Putkonen, A. Harlin, Atomic layer deposited thin barrier films for packaging, Cell. Chem. Technol. 49 (2015) 575–585. http://www.cellulosechemtechnol.ro/pdf/CCT7-8(2015)/p.575-585.pdf.
[109] S. Lange, T. Arroval, R. Saar, I. Kink, J. Aarik, A. Krumme, Oxygen barrier properties of Al_2O_3- and TiO_2-coated LDPE films, Polym. Plast. Technol. Eng. 54 (2015) 301–304, https://doi.org/10.1080/03602559.2014.977426.

[110] K. Kim, H. Luo, T. Zhu, O.N. Pierron, S. Graham, Influence of polymer substrate damage on the time dependent cracking of SiNx barrier films, Sci. Rep. 8 (2018) 4560, https://doi.org/10.1038/s41598-018-22105-2.
[111] R.L. Kovács, G. Langer, S. Gyöngyösi, Z. Erdélyi, A versatile technique for in situ investigation of the effect of thin film cracking on gas permeation of coated flexible polymers, Rev. Sci. Instrum. 92 (2021), 015120, https://doi.org/10.1063/5.0028783.
[112] Cs. Póliska, Z. Gácsi, P. Barkóczy, The effect of melt flow on the dendrite morphology, Mater. Sci. Forum. 508 (2006) 117–124, https://doi.org/10.4028/www.scientific.net/MSF.508.169.
[113] H. Klumbies, P. Schmidt, M. Hähnel, A. Singh, U. Schroeder, C. Richter, T. Mikolajick, C. Hoßbach, M. Albert, J.W. Bartha, K. Leo, L. Müller-Meskamp, Thickness dependent barrier performance of permeation barriers made from atomic layer deposited alumina for organic devices, Org. Electron. 17 (2015) 138–143, https://doi.org/10.1016/j.orgel.2014.12.003.
[114] R.L. Kovács, L. Daróczi, P. Barkóczy, E. Baradács, E. Bakonyi, S. Kovács, Z. Erdélyi, Water vapor transmission properties of acrylic organic coatings, J. Coat. Technol. Res. 18 (2021) 523–534, https://doi.org/10.1007/s11998-020-00421-5.
[115] G.B. Lee, K.S. Son, S.W. Park, J.H. Shim, B.-.H. Choi, Low-temperature atomic layer deposition of Al_2O_3 on blown polyethylene films with plasma-treated surfaces, J. Vac. Sci. Technol. 31 (2013) 01A129, https://doi.org/10.1116/1.4768171.
[116] R.L. Kovács, M. Csontos, S. Gyöngyösi, J. Elek, B. Parditka, G. Deák, Á. Kuki, S. Kéki, Z. Erdélyi, Surface characterization of plasma-modified low density polyethylene by attenuated total reflectance fourier-transform infrared (ATR-FTIR) spectroscopy combined with chemometrics, Polym. Test. 96 (2021), 107080, https://doi.org/10.1016/j.polymertesting.2021.107080.
[117] A. Gray, B.B. Mathews, T.M. MacRobert, A Treatise on Bessel Functions and Their Applications to Physics, Macmillan and Co., Ltd, London, 1931.
[118] R.B. Kelman, Steady-state diffusion through a finite pore into an infinite reservoir: an exact solution, Bull. Math. Biophys. 27 (1965) 57–65, https://doi.org/10.1007/BF02476468.
[119] P.O. Brunn, V.I. Fabrikant, T.S. Sankar, Diffusion through membranes: effect of a non-zero membrane thickness, Q. J. Mech. Appl. Math. 37 (1984) 311–324, https://doi.org/10.1093/qjmam/37.2.311.
[120] V.I. Fabrikant, On the potential flow through membranes, Journal of Applied Mathematics and Physics (ZAMP) 36 (1985) 616–623, https://doi.org/10.1007/BF00945301.
[121] V.I. Fabrikant, Diffusion through perforated membranes, J. Appl. Phys. 61 (1987) 813, https://doi.org/10.1063/1.338127.